

Self-diffusion and Cooperative Diffusion in Semidilute Polymer Solutions as measured by Fluorescence Correlation Spectroscopy

Ute Zettl¹, Sebastian T. Hoffmann¹, Felix Koberling², Georg Krausch³, Jörg Enderlein⁴, Ludger Harnau⁵, Matthias Ballauff^{1*}
¹*Physikalische Chemie I, University of Bayreuth, D-95440 Bayreuth, Germany*
²*Picoquant GmbH, D-12489 Berlin, Germany*
³*University of Mainz, Germany*

⁴*3. Institute of Physics, Georg August University, D-37077 Göttingen, Germany*

⁵*Max-Planck-Institut für Metallforschung, Heisenbergstr. 3, D-70569 Stuttgart, Germany,
 and Institut für Theoretische und Angewandte Physik,
 Universität Stuttgart, Pfaffenwaldring 57, D-70569 Stuttgart, Germany*

(Dated: January 10, 2022)

We present a comprehensive investigation of polymer diffusion in the semidilute regime by fluorescence correlation spectroscopy (FCS) and dynamic light scattering (DLS). Using single-labeled polystyrene chains, FCS leads to the self-diffusion coefficient while DLS gives the cooperative diffusion coefficient for exactly the same molecular weights and concentrations. Using FCS we observe a new fast mode in the semidilute entangled concentration regime beyond the slower mode which is due to self-diffusion. Comparison of FCS data with data obtained by DLS on the same polymers shows that the second mode observed in FCS is identical to the cooperative diffusion coefficient measured with DLS. An in-depth analysis and a comparison with current theoretical models demonstrates that the new cooperative mode observed in FCS is due to the effective long-range interaction of the chains through the transient entanglement network.

I. INTRODUCTION

Diffusion in polymer solutions is among the oldest subjects of polymer physics.^{1,2} In general, transport by diffusion can be characterized by two diffusion coefficients: the self-diffusion coefficient D_s and the cooperative diffusion coefficient D_c . D_s describes the motion of one molecule relative to the surrounding molecules due to thermal motions while D_c describes the motion of a number of molecules in a density gradient.³⁻⁷ The obvious importance of diffusion in polymer physics has led to a rather large number of studies of D_c by dynamic light scattering (DLS),³⁻⁹ while D_s can be obtained by pulsed-field gradient nuclear magnetic resonance^{4,6,7} and label techniques like forced Rayleigh scattering¹⁰ or fluorescence correlation spectroscopy (FCS).¹¹⁻¹³ However, in many cases D_s and D_c could not be obtained for the same homopolymer using the same technique. Such measurements would be very interesting since a central problem in the dynamics of semidilute entangled polymer solutions is the quantitative understanding of the interplay of self-diffusion and cooperative diffusion. Very recently it has been found theoretically that the coupling of self- and cooperative motion due to topological constraints is also important for rather stiff macromolecules.¹⁴

At present, DLS is certainly among the most accurate methods to measure D_c and there is a number of careful studies conducted on polymer solutions. In principle, FCS is the method of choice for studying diffusion of single macromolecules in a matrix of same molecular weight giving D_s or in a solution of polymers of different molecular weight (tracer diffusion¹⁵⁻¹⁷). In opposite to DLS, FCS requires chains labeled by a stable fluorescing molecule. Moreover, the number of labels per macro-

molecules should be constant to arrive at results that can be directly compared to theory. Given these problems, the use of FCS for measurements of D_s on synthetic polymers has been scarce so far.^{11-13,18} Moreover, the full potential of this method has not yet fully been exploited yet since FCS should also allow one to obtain D_c .^{19,20}

Recently, a well-defined polymeric model system has been presented and used for quantitative FCS-measurements in dilute solution.^{11,12} Nearly monodisperse polystyrene chains have been prepared by anionic polymerization and subsequently labeled by single fluorescent dye. Since the molecular weight of the different samples span a wide range, these polymers provide a nearly ideal model system for exploring the chain dynamics over a wide range of molecular weights and concentrations. Using these labeled chains, we recently presented an in-depth study of the experimental FCS set-up¹¹ as well as of the dynamics in dilute solution.¹²

Here we pursue these studies further by presenting an investigation of polymer diffusion in the semi-concentrated regime by FCS. In order to obtain accurate data of cooperative diffusion, these studies are combined with DLS-measurements on exactly the same molecular weights and concentrations. Thus, D_c and D_s can now be obtained from identical systems and directly be compared. In the course of these studies we found that a second cooperative mode becomes visible in the FCS-experiments if the concentration exceeds a given value. This surprising finding prompted us to conduct a full theoretical analysis of both the FCS- as well as of the DLS-data throughout the entire time scale and range of concentrations available by these experiments. In doing so we extend the theoretical modeling beyond the usual scaling laws. The entire study is devoted to a comprehensive

understanding of polymer dynamics in solution ranging from the dilute state up to the onset of glassy dynamics.

The paper is organized as follows: After the Section Experimental we first present the FCS-data together with the finding of the new cooperative diffusion. In the subsequent section a quantitative modeling of the data in terms of an analytical theory will be given. In the last section special attention will be paid to possible practical applications of these findings to the spinning of nanofibers. A Conclusion will wrap up the entire discussion.

II. EXPERIMENTAL SECTION

A. Dye Labeled Polystyrene

All experiments reported here were carried out with linear polystyrenes having a narrow molecular weight distribution. For details of the synthesis see ref¹¹. The molecular weight and polydispersity of the polymers are summarized in Table I. The solutions for the FCS experiments were prepared in toluene p. a. grade by blending a constant concentration of 10^{-8} M Rhodamine B labeled polystyrene with varying amounts of unlabeled polystyrene from the same synthesis batch. Each labeled polymer carries only one dye molecule at one of its ends. To verify our results, additional solutions were prepared with varying labeled polystyrene and a constant amount of unlabeled polystyrene. We have used preparative gel permeation chromatography to separate labeled polymer and free dye molecules.^{11,21} Therefore, the resulting dye-labeled polymer does not contain any measurable amount of free dye molecules.

TABLE I: Molecular weight M_w , polydispersity index $PDI=M_w/M_n$ and hydrodynamic radius R_h at infinite dilution of the polystyrenes used in the present study. The second and the third virial coefficients A_2 and A_3 , respectively, have been calculated using scaling laws taken from the literature (A_2 : ref²² and A_3 : ref⁹). c^+ is the concentration at which the second diffusion time appears in the FCS measurements.

$M_w[\frac{kg}{Mol}]$	PDI	$R_h[nm]$	$A_2[\frac{cm^3 Mol}{g^2}]$	$A_3[\frac{cm^6 Mol}{g^3}]$	$c^+[wt\%]$
11.5	1.03	1.(4)	$7.4 \cdot 10^{-4}$	$2.1 \cdot 10^{-3}$	-
17.3	1.03	1.(6)	$6.8 \cdot 10^{-4}$	$2.6 \cdot 10^{-3}$	-
67.0	1.05	3.(9)	$5.1 \cdot 10^{-4}$	$5.8 \cdot 10^{-3}$	20
264	1.02	7.(3)	$3.8 \cdot 10^{-4}$	$1.3 \cdot 10^{-2}$	6.5
515	1.09	9.(8)	$3.3 \cdot 10^{-4}$	$1.9 \cdot 10^{-2}$	4.8

B. Methods

For FCS measurements we modified the commercial ConfoCor2 setup (Carl Zeiss, Jena, Germany)²³

with a 40× Plan Neofluar objective (numerical aperture NA=0.9). The Rhodamine B labeled PS-chains were excited by a HeNe-Ion laser at 543 nm. The intensity for all measurements was 4μW in sample space. As second setup we used a MicroTime200 (PicoQuant, Berlin, Germany)²⁴ with a 100× oil immersion objective (NA=1.45). Here the detection beam path was divided by a 50/50 beam splitter on two detectors to crosscorrelate the signals. This crosscorrelation is necessary to prevent distortion of the fluorescence correlation function by detector afterpulsing.²⁵ For details of the FCS-measurements see refs^{11,12,23}.

Cooperative diffusion coefficients D_c were measured by DLS using an ALV 4000 light scattering goniometer (Peter, Germany).

C. Evaluation of Data

In FCS^{23,26} a laser beam is focused by an objective with high numerical aperture (typically ≥ 0.9) and excites fluorescent molecules entering the illuminated observation volume. The emitted fluorescent light is collected by the same optics and separated from scattered light by a dichroic mirror. The emitted light is detected by an avalanche photo diode. The time dependent intensity fluctuations $\delta I(\tau) = I(\tau) - \langle I(\tau) \rangle$ are analyzed by an autocorrelation function, where $\langle \rangle$ denotes an ensemble average. This autocorrelation function can be written as²⁰

$$G(\tau) = \frac{1}{N} \int d\mathbf{q} \Omega(\mathbf{q}) C(\mathbf{q}, \tau) \quad (1)$$

where $\Omega(\mathbf{q}) = \pi^{-\frac{3}{2}} w_{x,y}^2 w_z \exp(-w_{x,y}^2 (q_x^2 + q_y^2)/4 - w_z^2 q_z^2/4)$ is a Gaussian filter function characterizing the observation volume in Fourier space with $\int d\mathbf{q} \Omega(\mathbf{q}) = 1$, N is the average number of fluorescently labeled molecules in the observation volume, and $\mathbf{q} = (q_x, q_y, q_z)$. Here $w_{x,y} = 296$ nm is the dimension of the observation volume perpendicular to the optical axis and $w_z = 8w_{x,y}$ is the dimension along the optical axis.^{11,12} For an ideal gas consisting of non-interacting molecules the initial amplitude reduces to the familiar relationship $G(0) = 1/N$.²³

The time-dependent fluorescence density-density autocorrelation function $C(\mathbf{q}, \tau)$ is expressed in terms of a coupled-mode model^{27,28} as

$$C(\mathbf{q}, \tau) = \frac{C_c(q, 0)e^{-q^2 \phi_c(\tau)/6} + C_s(q, 0)e^{-q^2 \phi_s(\tau)/6}}{C_c(q, 0) + C_s(q, 0)} \quad (2)$$

where $q = |\mathbf{q}|$. Here the mean square displacements $\phi_c(\tau)$ and $\phi_s(\tau)$ are given by

$$\phi_c(\tau) = 6D_c\tau, \quad (3)$$

$$\phi_s(\tau) = 6D_s\tau + B_s(\tau). \quad (4)$$

The term $B_s(\tau)$ allows one to take into account the contributions from internal polymer chain motions.² If

only a few of the molecules are fluorescently labeled, the self-diffusion coefficient D_s can be measured in the FCS experiment.¹² If all of the molecules are fluorescently labeled, the cooperative diffusion coefficient D_c can be obtained.¹⁹ In the case that neither of these limits applies, both the self mode and the cooperative mode will be present in the spectrum of the autocorrelation function. The diffusion coefficients can be extracted by fitting

$$G(\tau) = \sum_{i \in \{s, c\}} G_i(0) \left(1 + \frac{2\phi_i(\tau)}{3w_{x,y}^2}\right)^{-1} \left(1 + \frac{2\phi_i(\tau)}{3w_z^2}\right)^{-1/2} \quad (5)$$

to the experimental data. FCS is not only sensitive to intensity fluctuations due to the motion of labeled molecules but also due to photokinetic processes of the fluorescent dyes which occur for short times $\tau \lesssim 5 \times 10^{-3}$ ms. This additional relaxation has been taken into account as discussed in refs^{11,12,21}.

DLS allows one to measure the time dependent autocorrelation function of the scattered electric field which can be expressed in terms of the elements of the fluid polarizability tensor.⁸ For an incident light wave traveling in the x direction with a polarization vector in the z direction the intensity of the scattered electric field can be written as

$$I_{VV}(\mathbf{q}, \tau) \sim \int d\mathbf{r} d\mathbf{r}' \langle \alpha_{zz}(\mathbf{r} + \mathbf{r}', \tau) \alpha_{zz}(\mathbf{r}', 0) \rangle e^{i\mathbf{q} \cdot \mathbf{r}}, \quad (6)$$

where the absolute value of the scattering vector \mathbf{q} is given by $q = |\mathbf{q}| = (4\pi n/\lambda) \sin(\theta/2)$ in which n is the refractive index of the medium. λ is the incident wavelength and θ is the scattering angle. The zz element of the fluid polarizability tensor is denoted as $\alpha_{zz}(\mathbf{r}, \tau)$. The experimentally accessible quantity is the intensity autocorrelation function $g_{VV}^{(2)}(\mathbf{q}, \tau)$. For photon counts obeying Gaussian statistics, the intensity autocorrelation function is related to the electric field autocorrelation function $g_{VV}^{(1)}(\mathbf{q}, \tau)$ according to

$$g_{VV}^{(2)}(\mathbf{q}, \tau) = 1 + f_{VV} \left(g_{VV}^{(1)}(\mathbf{q}, \tau) \right)^2, \quad (7)$$

where f_{VV} is dependent on the scattering geometry. The electric field correlation function can be calculated for various systems. For a solution containing purely diffusing particles the electric field correlation function is given by $g_{VV}^{(1)}(q, \tau) = \exp(-q^2 D_c \tau) / \sqrt{f_{VV}}$.

III. DIFFUSION COEFFICIENTS MEASURED BY FCS

Figure 1 shows normalized autocorrelation functions measured by FCS. The average number of labeled polymers in the observation volume was kept constant to

$N \approx 0.8$ whereas the number of unlabeled polymers increases up to $N_u = 3 \times 10^6$ for the 28 wt % polymer solution. The thin broken curves are measured at the ConfoCor2 setup and the thick solid curve is measured at the MicroTime200 setup. The curves obtained at the ConfoCor2 setup have an additional decay on the time scale less than $10 \mu s$. This additional decay belongs to detector afterpulsing. Hence, the evaluation of the correlation curves has been done only for $\tau \geq 10 \mu s$ as indicated by the dotted line in Figure 1. For low polymer concentrations we obtained correlation curves with a single diffusion time. With increasing polymer concentration the correlation curves shift to higher diffusion times.

As an entirely new finding, Figure 1 presents a new mode related to a second diffusion time measured with FCS at higher polymer concentrations. This second diffusion time appears at shorter time scales than the one related to self-diffusion. The concentration c^+ at which the second diffusion time is detected depends on the molecular weight: The higher the molecular weight, the lower is c^+ (see Table I). In general c^+ is about $15\times$ the overlap concentration determined in an earlier study.¹² For the concentration c^+ the ratio between these two diffusion times is in the range of 60. From both diffusion times we calculated the diffusion coefficients from the relations given above.

In Figures 2 and 3 all diffusion coefficients measured with FCS and DLS are compared at identical conditions. At infinite dilution both diffusion coefficients D_s and D_c have the same value. In dilute solutions D_s and D_c show a linear dependency on the concentration as expected according to the Kirkwood-Riseman theory.²⁹ But D_s decreases whereas D_c increases with increasing polymer

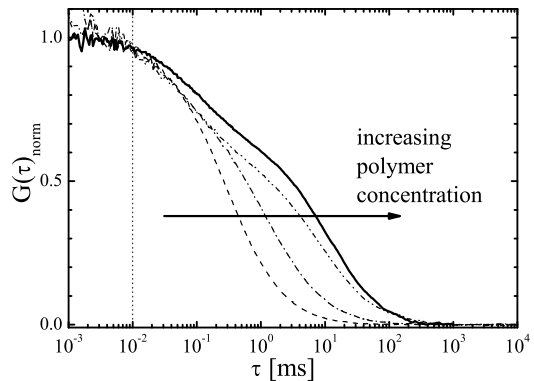


FIG. 1: Normalized autocorrelation function obtained from FCS for polystyrene of molecular weight $M_w = 67$ kg/Mol in toluene for various polymer concentrations: 0.03 wt% (—), 9.1 wt% (— · —), 20 wt% (— · —) and 28 wt% (—). A second diffusion time appears at 20 wt% on a shorter timescale compared to self-diffusion. The thick solid line is the normalized crosscorrelation curve without detector afterpulsing for the 28 wt% polymer solution. The dotted vertical line marks the time scale above which this artefact becomes negligible, i.e., the solid thin and thick lines coincide for $\tau > 0.01$ ms.

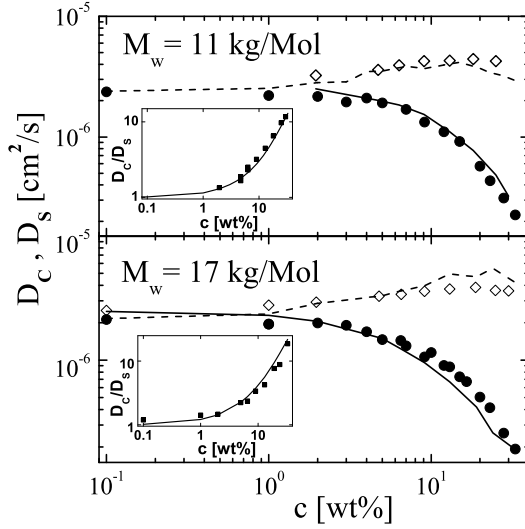


FIG. 2: Comparison of self-diffusion coefficients (D_s , ●) with cooperative diffusion coefficients (D_c , ◇) for different molecular weights: $M_w = 11$ and 17 kg/Mol (top and bottom). Open and solid symbols refer to DLS and FCS measurements, respectively. The solid lines represent D_s calculated according to eq 8 with D_c as input from DLS measurements. The dashed lines represent D_c calculated vice versa, i.e., with D_s as input from FCS experiments. Insets: Measured ratio D_c/D_s (symbols) together with the corresponding ratio obtained from eqs 8 and 9 within a third order virial approximation (see Table I).

concentration. The decrease of D_s is due to the friction between the chains and the increase of D_c is due to the increasing osmotic pressure.^{30,31} At high concentrations D_c exhibits a maximum.

The insets in Figure 2 and Figure 3 show the ratio D_c/D_s of measured values. The lines are theoretical values calculated according to^{6,7}

$$\frac{D_c}{D_s} = (1 - \bar{v}c) \frac{d\Pi}{dc} \quad (8)$$

with the partial specific volume of the polymer \bar{v} and the polymer concentration c . The dependence of the osmotic pressure on c can be approximated by a virial expansion

$$\frac{d\Pi}{dc} = 1 + 2A_2M_w c + 3A_3M_w c^2 + \dots, \quad (9)$$

where A_2 and A_3 are the second and third virial coefficients, respectively, and M_w is the molecular weight. For the calculation of $d\Pi/dc$ we used the corresponding values from the literature gathered in Table I and $\bar{v} = 0.916$ cm³/g.³² The measured and the calculated ratio are well described as demonstrated by the inset of Figures 2 and 3. The self-diffusion coefficients D_s can be determined from the cooperative diffusion coefficient D_c obtained by DLS measurements and vice versa. D_s and D_c can be measured with high accuracy by FCS and

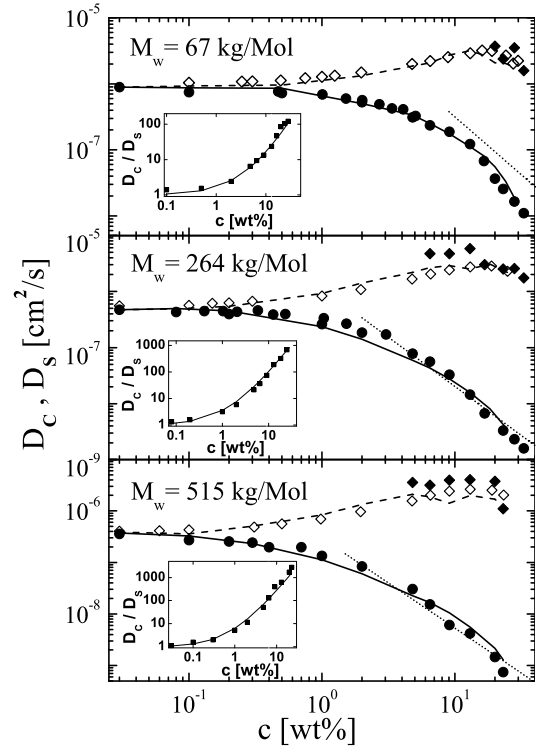


FIG. 3: Comparison of self-diffusion coefficients (D_s , ●) with cooperative diffusion coefficients (D_c , ◆, ◇) for different molecular weights: $M_w = 67$, 264 and 515 kg/Mol (from top to bottom). Open and solid symbols refer to DLS and FCS measurements, respectively. The solid lines represent D_s calculated according to eq 8 with D_c as input from DLS measurements. The dashed lines represent D_c calculated vice versa, i.e., with D_s as input from FCS experiments. For comparison the dotted lines represent the scaling prediction $D_s \sim M_w^{-2} c^{-7/4}$ for long polymer chains in the semidilute entangled regime (see eq 12). Insets: Measured ratio D_c/D_s (symbols) together with the corresponding ratio obtained from eqs 8 and 9 within a third order virial approximation (see Table I).

DLS using the same polymers. Their relation is fully understood in terms of eq 8. For comparison we note that both the molecular dye diffusion coefficient and the macromolecular tracer diffusion coefficient decrease with increasing concentration of the matrix polymer.¹⁷

Figure 4 displays the amplitudes $G_i(0)$ (see eq 5) as a function of N for polystyrene with $M_w = 67$ kg/Mol at 20 wt%. The amplitude of the self-diffusion mode $G_s(0)$ is proportional to $1/N$. In the presence of non-correlated background signal (scattering, afterpulsing, electronic noise) this is modified to $1/N - 2b/N^2$.²³ Here b is proportional to the noise intensity, which is assumed to be significantly smaller than the fluorescence signal. For the cooperative mode one finds an amplitude scaling of $1 - 2bN$. For sufficiently small b , this will yield a dependence as shown by Figure 4 for the fast correlation component.

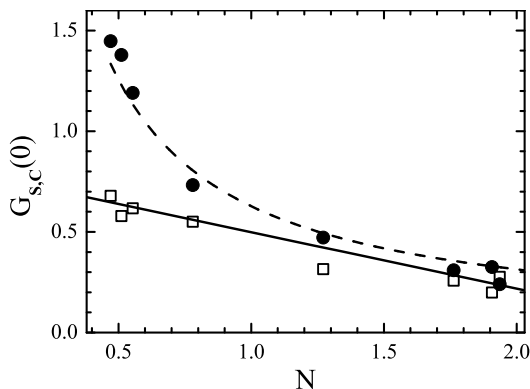


FIG. 4: Amplitudes $G_s(0)$ (●) and $G_c(0)$ (□) extrapolated from the measured FCS-autocorrelation function $G(\tau)$ as a function of labeled molecules N for polystyrene with $M_w = 67$ kg/Mol at 20 wt%. For the self-diffusion $G_s(0) \propto 1/N$ (---), while $G_c(0)$ exhibits a linear dependence on N (—) for the cooperative diffusion.

The ratio $G_c(0)/G(0)$ is a non-monotonic function of the concentration for a fixed number of labeled molecules N . It increases from 0 to a value below 1 at the concentration c^+ . $G_c(0)/G(0)$ slightly decreases upon further increasing the concentration in the semidilute entangled regime. Finally, it increases upon approaching the glass transition concentration.

IV. SCALING THEORY AND LANGEVIN EQUATION APPROACH

In the following section, the findings presented in the previous sections will be compared to current models of polymer diffusion.

A. Scaling theory and reptation model

The application of scaling theory and the reptation model to polymer solutions has been presented in various treatises (see, e.g., refs^{1,2,33,34}). Hence, we only discuss the equations necessary for this study. Three concentration regimes can be distinguished: dilute, semidilute unentangled, and semidilute entangled solutions. Scaling arguments and the reptation model lead to following relations for the self-diffusion coefficient D_s and the cooperative diffusion coefficient D_c :

$$D_s = D_c \sim M_w^{-3/5} c^0, \quad c \ll c^*, \quad (10)$$

$$D_c \sim M_w^0 c^{3/4}, \quad c > c^*, \quad (11)$$

$$D_s \sim M_w^{-2} c^{-7/4}, \quad c > c^{**}. \quad (12)$$

Here the overlap concentration c^* is the boundary concentration between the dilute and semidilute regimes.

This concentration depends on molecular weight as

$$c^* \sim M_w^{1-3\nu} = M_w^{-4/5}, \quad (13)$$

where the Flory exponent $\nu = 3/5$ for a good solvent has been used. The crossover concentration from the semidilute unentangled to the semidilute entangled regime is denoted as c^{**} .

For very low concentrations in the dilute regime, the self-diffusion coefficient is indistinguishable from the cooperative diffusion coefficient as is apparent from Figures 2 and 3. In Figure 5 the self-diffusion coefficient is plotted as a function of the molecular weight M_w for a fixed concentration $c = 9.1$ wt %. The experimental data (solid squares) follow the scaling laws given by eq 10 (dashed line) and eq 12 (solid line) for $M_w \leq 20$ kg/Mol and $M_w \geq 264$ kg/Mol, respectively. Moreover, D_s is rather independent of concentration for $c \lesssim 10$ wt % in the case of the low molecular weight solution (see Figure 2 and eq 10). The concentration dependence of D_s of the higher molecular weight solutions ($M_w \geq 264$ kg/Mol) is in accord with the scaling prediction for the reptation model (eq 12) which is represented in Figure 3 by the dotted lines. Hence the FCS measurements verify the basic scaling and reptation theory for semidilute entangled polymer solutions similar to earlier forced Rayleigh scattering experiments of polystyrene in benzene.^{10,35}

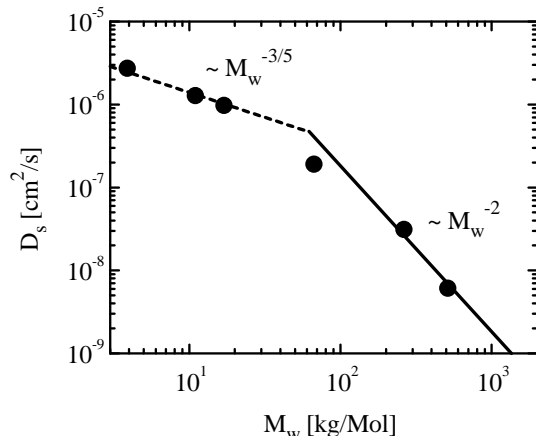


FIG. 5: The self-diffusion coefficient D_s (●) measured by FCS at the fixed concentration $c = 9.1$ wt % as a function of the molecular weight M_w . The dashed and solid lines of slope $M_w^{-3/5}$ (see eq 10) and M_w^{-2} (see eq 12), respectively, represent two asymptotic scaling regimes.

In the limit $c \rightarrow 0$ the experimental data follow the scaling law given by eq 10 irrespective of the molecular weight,¹² i.e., also the higher molecular weight PS solutions obey the scaling relation $D_s \sim M_w^{-3/5} c^0$. This result is in agreement with earlier quasi-elastic light scattering experiments for polystyrene in 2-butanone³⁶ or in benzene.³

B. Internal motions of chains

In order to examine the influence of internal chain motions such as bending and stretching on the dynamics (see refs^{37–40} and references therein), one may trace out the internal degrees of freedom of a polymer chain by studying the monomer mean square displacement $B_s(\tau)$ in eq 4 in detail. Various theoretical predictions on the time dependence of the monomer mean square displacement of both continuously and single labeled DNA molecules in aqueous solution have been verified using FCS measurements.^{41–46} In these earlier experimental and theoretical studies the Θ condition has been considered. However, for PS in toluene solutions the intramolecular excluded volume interaction has to be taken into account. In this case scaling arguments^{47,48} lead to the following time dependence of the monomer mean square displacement:

$$B_s(\tau) = B_s \tau^{1/(1+1/(2\nu))} = B_s \tau^{6/11}. \quad (14)$$

It proves convenient to consider the function $1/G(\tau) - 1$, which amplifies the time dependence of $G(\tau)$ for small times, because $w_z^2 = 64w_{x,y}^2$ in eq 5.⁴⁵ If the autocorrelation function $G(\tau)$ exhibits a time dependence according to eqs 4, 5, and 14 with $G_c(0) = 0$, a double logarithmic plot will directly yield the exponent $1/(1 + 1/(2\nu))$ for small times provided the intramolecular dynamics dominates, i.e., $B_s(\tau) \gg 6D_s\tau$.

Figure 6 shows such a representation of the autocorrelation function for the 515 kg/Mol PS chains in dilute solution. The experimental data (solid squares) follow the scaling law given by eq 14 (dotted line) and the diffusive behavior (lower dashed line) for short and large times, respectively. Hence for short times the decay of the autocorrelation function is dominated by intramolecular chain relaxations, while self-diffusion dominates for large times. Figure 6 demonstrates that the measured autocorrelation function agrees with the calculated results (solid line) obtained from eqs 4, 5, and 14 with D_s and B_s as input. The mean displacements $\sqrt{\phi_s(\tau)}$ as calculated from eq 5 with $G_s(0) = 1$ and $G_c(0) = 0$ are given by 131 nm and 598 nm for $\tau = 0.01$ ms and $\tau = 1$ ms, respectively.

It is apparent from Figure 6 that the contribution of internal chain motions cannot be observed in the case of the 17 kg/Mol PS chains in dilute solution (solid triangles) because of the dominating diffusive motion (upper dashed line). The self-diffusion coefficient D_s increases upon decreasing molecular weight according to eq 10, while B_s is less dependent on molecular weight. Finally, it is worthwhile to mention the contribution of internal chain motions to the dynamics decreases upon increasing the polymer concentration because of the presence of the surrounding polymer chains.^{47,49}

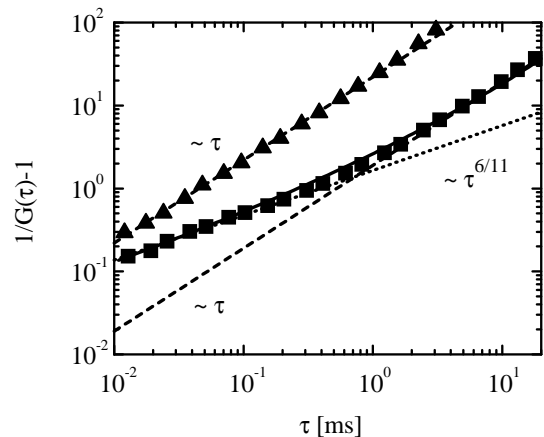


FIG. 6: The autocorrelation function $1/G(\tau) - 1$ of a 515 kg/Mol (■) and a 17 kg/Mol (▲) polystyrene solution measured by FCS in the limit $c \rightarrow 0$ as a function of the time τ . The dotted and dashed lines of slope $\tau^{6/11}$ (see eq 14) and τ (see eq 4), respectively, represent two asymptotic scaling regimes. The solid line displays the result for the 515 kg/Mol polystyrene solution as obtained from eq 5 with eqs 4 and 14 as input. The autocorrelation function of the 17 kg/Mol polystyrene solution (▲ and upper dashed line) is shifted up by a factor of 2.

C. Cooperative diffusion

We now turn our attention to the scaling law for the cooperative diffusion coefficient given by eq 11. Figure 7 displays the cooperative diffusion coefficient D_c of the 515 kg/Mol PS solution (solid squares) together with the scaling law (dashed line) as a function of the concentration. Several experimental measurements have yielded the concentration dependence $D_c \sim c^{0.65}$ instead of the scaling prediction $D_c \sim c^{3/4} = c^{0.75}$.^{3,50–53} Various possible explanations for these deviations from the scaling law have been discussed,^{54,55} such as the counter-motion of the solvent induced by the motion of the polymers. On the basis of our results shown in Figure 7 we note that the transition between the dilute regime with $D_c \sim c^0$ (dotted line and eq 10) and the semidilute unentangled regime with $D_c \sim c^{3/4}$ (dashed line and eq 11) is not so abrupt, as has been assumed by scaling theories, but is a rather smooth crossover that extends over more than one order in magnitude of concentration.

It has been emphasized that it would be desirable to model the dynamics both in the dilute regime and the semidilute regimes explicitly within one theoretical approach.³³ Successful models should incorporate the transition region between the dilute regime and the semidilute regimes. In the next subsection we provide a quantitative basis for such a modelling of cooperative dynamical properties of polymer chains in good solution.

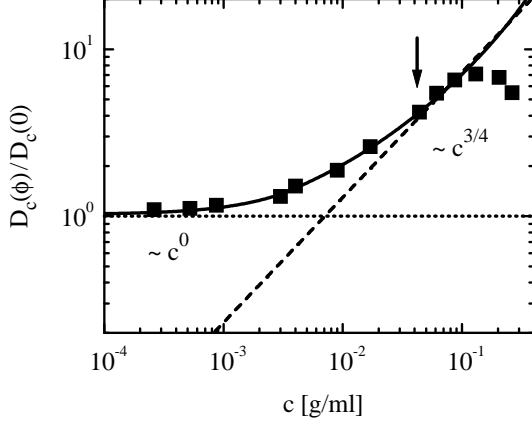


FIG. 7: The normalized cooperative diffusion coefficient D_c (■; DLS) of a 515 kg/Mol polystyrene solution as a function of the concentration c . The dashed and dotted lines of slope $c^{3/4}$ (see eq 11) and c^0 (see eq 10), respectively, represent two asymptotic scaling regimes. The solid line displays the results as obtained from the Langevin and generalized Ornstein-Zernike equation according to eqs 17 - 23. The arrow marks the location of the concentration $c^+ = 0.044$ g/ml at which the cooperative diffusion mode appears in the FCS measurements (see Figure 3).

D. Analytical theory: Langevin and generalized Ornstein-Zernike equation

We consider a monodisperse polymer solution consisting of $N_{tot} = N + N_u$ polymer chains and the solvent. Each polymer chain carries n scattering units. The total dynamic scattering function $S_{tot}(q, \phi, \tau)$ is defined as

$$S_{tot}(q, \phi, \tau) = \frac{1}{N_{tot} n^2} \left\langle \sum_{\alpha, \gamma=1}^{N_{tot}} \sum_{j, k=1}^n e^{i\mathbf{q} \cdot (\mathbf{r}_{\alpha j}(\tau) - \mathbf{r}_{\gamma k}(0))} \right\rangle, \quad (15)$$

where $q = |\mathbf{q}|$ is the magnitude of the scattering vector \mathbf{q} and $\langle \rangle_\phi$ denotes an ensemble average for a given polymer volume fraction ϕ . Here $\mathbf{r}_{\alpha j}(\tau)$ is the position vector of the j -th scattering unit ($1 \leq j \leq n$) of the α -th particle ($1 \leq \alpha \leq N_{tot}$) at time τ . The normalized total dynamic scattering function is related to the electric field autocorrelation function measured by DLS according to $S_{tot}(q, \phi, \tau)/S_{tot}(q, \phi, 0) = g_{VV}^{(1)}(q, \tau)\sqrt{f_{VV}}$. (see eq 7). The time evolution of the total dynamic scattering function is assumed to be governed by the Langevin equation²

$$\frac{d}{d\tau} S_{tot}(q, \phi, \tau) = -\Gamma(q, \phi) S_{tot}(q, \phi, \tau). \quad (16)$$

The validity of this equation is not obvious since entanglements have not been taken into account in the derivation of this equation.² However, the short time-scale dynamics can be described by eq 16 since the topological

constraints are not so important in the short time-scale dynamics as is apparent from the fact that the cooperative diffusion coefficient D_c is considerably larger than the self-diffusion coefficient D_s in the semidilute entangled regime (see Figure 3). The decay rate $\Gamma(q, \phi)$ is given by²

$$\Gamma(q, \phi) = \frac{k_B T}{4\pi^2 \eta} \int_0^\infty dq_1 q_1^2 \frac{S_{tot}(q_1, \phi, 0)}{S_{tot}(q, \phi, 0)} \left(\frac{q_1^2 + q^2}{2q_1 q} \log \left| \frac{q_1 + q}{q_1 - q} \right| - 1 \right), \quad (17)$$

where the temperature T and the viscosity η characterize the solvent. The volume fraction-dependent cooperative diffusion coefficient $D_c(\phi)$ can be calculated according to

$$D_c(\phi) = \lim_{q \rightarrow 0} \frac{\Gamma(q, \phi)}{q^2}. \quad (18)$$

Furthermore, the total static scattering function reads

$$S_{tot}(q, \phi, 0) = 1 + \phi h(q, \phi)/(V_p P(q, \phi)), \quad (19)$$

where V_p is the volume of a dissolved polymer chain and $h(q, \phi)$ is a particle-averaged total correlation function. The particle-averaged intramolecular correlation function

$$P(q, \phi) = \frac{1}{N_{tot} n^2} \left\langle \sum_{\alpha=1}^{N_{tot}} \sum_{j, k=1}^n e^{i\mathbf{q} \cdot (\mathbf{r}_{\alpha j}(0) - \mathbf{r}_{\alpha k}(0))} \right\rangle, \quad (20)$$

characterizes the geometric shape of the polymer chains at a given volume fraction ϕ . While the particle-averaged intramolecular correlation function accounts for the interference of radiation scattered from different parts of the same polymer chain in a scattering experiment, the local order in the fluid is characterized by $h(q, \phi)$. The particle-averaged total correlation function is related to a particle-averaged direct correlation function $c(q, \phi)$ by the generalized Ornstein-Zernike equation of the Polymer Reference Interaction Site Model (PRISM), which reads (see refs⁵⁶⁻⁵⁸ and references therein)

$$h(q, \phi) = P^2(q, \phi) c(q, \phi) / (1 - \phi c(q, \phi) P(q, \phi) / V_p). \quad (21)$$

This generalized Ornstein-Zernike equation must be supplemented by a closure relation. If the interaction sites are simply the centers of exclusion spheres, to account for steric effects, a convenient closure is the Percus-Yevick approximation.⁵⁶ The PRISM integral equation theory has been successfully applied to various experimental systems such as polymers,^{56,59} bottle-brush polymers,^{60,61} rigid dendrimers,^{62,63} and charged colloids.⁶⁴⁻⁷¹

The overall size of the polymer chains is reduced considerably upon increasing the volume fraction implying a concentration dependence of the particle-averaged intramolecular correlation function $P(q, \phi)$. Therefore, we

consider the following particle-averaged intramolecular correlation function⁷²

$$P(q, \phi) = (1 + 0.549 q^2 r_g^2(\phi))^{-5/6} \quad (22)$$

with the volume fraction dependent radius of gyration

$$r_g^2(\phi) = \begin{cases} r_g^2(0) & , \quad c < c^* \\ r_g^2(0) \left(\frac{c}{c^*}\right)^{-1/8} & , \quad c > c^* \end{cases} \quad (23)$$

Here the relation between the volume fraction ϕ and the concentration c is given by $\phi = \bar{v}c$, where $\bar{v} = 0.916 \text{ cm}^3/\text{g}$ is the specific weight of PS.³² The scaling law given by eq 23 has been confirmed experimentally for PS in a good solvent using small angle neutron scattering.⁷³

Figure 7 demonstrates that the measured cooperative diffusion coefficients (solid squares) agree with the calculated results (solid line) obtained from eqs 17 - 23 both in the dilute and semidilute regimes. In particular, the features of the broad crossover region between the dilute and the semidilute regimes are captured correctly by the integral equation theory. In the calculations the model parameter $c^* = 0.0032 \text{ g/ml}$ ¹² and $r_g(0) = 32.8 \text{ nm}$ for the 515 kg/Mol PS solution has been used. This radius of gyration is about 6 % larger than corresponding radii of gyration of PS in various good solvents.^{9,22,74,75} The deviation between the radius of gyration used in the calculations and the radii of gyration reported in the literature might be due to the fact that the hydrodynamic interaction has been taken into account in terms of the Oseen tensor in order to derive eq 17. Using the Rotne-Prager tensor^{76,77} as a first correction to the Oseen tensor will improve the results. Moreover, the size polydispersity $M_w/M_n = 1.09$ of the 515 kg/Mol PS solution leads to a diffusion coefficient which is characteristic for monodisperse polymers of larger radius of gyration.⁷⁸

Finally, we note that the maximum of D_c in the semidilute entangled regime marks the onset of glassy dynamics which is discussed in ref⁵³. The friction-controlled dynamics in this concentration regime is not captured by eqs 16 and 17 and will be discussed in subsection IV F.

E. Coupling of cooperative fluctuations with single polymer chain motion

In the following we shall discuss the equation of motion which determines the dynamics an individual polymer chain. The PS chains are linear chain molecules which are described by a chain model for macromolecules.^{37,38,77} We consider a continuous, differentiable space curve $\mathbf{r}(s, \tau)$, where $s \in [-L/2, L/2]$ is a coordinate along the macromolecule and $\mathbf{r}(L/2, \tau)$ is the position vector of the labeled end monomer. The Langevin equation of motion

including hydrodynamic interaction is given by⁷⁷

$$3\pi\eta \frac{\partial}{\partial \tau} \mathbf{r}(s, \tau) = \int_{-L/2}^{L/2} ds' (3\pi\eta H(s-s') + \delta(s-s')) \times (O(s')\mathbf{r}(s', \tau) + \mathbf{f}(s', \tau)) + \mathbf{F}(s, \tau), \quad (24)$$

with

$$O(s) = 3k_B T p \frac{\partial^2}{\partial s^2} - \frac{3k_B T}{4p} \frac{\partial^4}{\partial s^4}. \quad (25)$$

Here $1/(2p)$ is the persistence length, $H(s-s')$ is the hydrodynamic interaction tensor, and $\mathbf{f}(s, \tau)$ is the stochastic force. The force $\mathbf{F}(s, \tau)$ describes the influence of intermolecular forces and is discussed below. The numerical solution of eq 24 allows one to calculate the mean square displacement (see eq 4) according to

$$\phi_s(\tau) = \left\langle (\mathbf{r}(L/2, \tau) - \mathbf{r}(L/2, 0))^2 \right\rangle. \quad (26)$$

This chain model has been used in the limit $\mathbf{F}(s, \tau) = 0$ in order to describe FCS measurements of DNA molecules in dilute solution.⁴³⁻⁴⁵ In particular, the model predicts the observed crossover from subdiffusive motion ($B_s(\tau)$ in eq 4) to diffusive motion ($6D_s\tau$ in eq 4) upon increasing the time τ . Moreover, it has been shown that the chain ends are more mobile than the central part of the polymer chain for short times.⁴⁵ For comparison we note that the quantity $\phi_s(\tau)$ contributes to the so called incoherent dynamic structure factor which is accessible by quasielastic neutron scattering (see ref⁷⁹ and references therein).

The key physics determining the dynamics of chain molecules in semidilute entangled solution arises from the intermolecular interaction which are taken into account in terms of the force $\mathbf{F}(s, \tau)$ in eq 24. Various expressions for the force $\mathbf{F}(s, \tau)$ have been proposed (see, e.g., refs⁸⁰⁻⁸⁸). These earlier theoretical considerations have demonstrated the coupling of cooperative fluctuations with single polymer chain motion in the semidilute entangled regime. This coupling allows one to measure D_c from the dynamics of individual labeled polymer chains with FCS. Hence, it provides the explanation for the finding of a cooperative mode in the FCS-experiment. The topological interaction in semidilute entangled polymer solutions seriously affects dynamical properties since it imposes constraints on the motion of the polymers. When the motion of a single polymer chain is partly hindered by the presence of other chains the cooperative diffusion becomes highly correlated and can be studied using only a small fraction of labeled molecules. Moreover, the number of molecules statistically involved in the correlated dynamics increases considerably upon approaching the glass transition concentration.

Figures 8 (a) and (b) display the function $1/G(\tau)-1$ for the 17 kg/Mol PS chains and the 515 kg/Mol PS chains in dilute solution (solid squares, $c \rightarrow 0$) and in semidilute solution (solid triangles, $c = 13 \text{ wt } \%$). For the 17

kg/Mol PS chains only self-diffusion can be measured using FCS irrespective of the concentration (see Figure 8 (a)) because of insufficient chain overlap. In the case of the 515 kg/Mol PS chains self-diffusion dominates for large times as is indicated by the dashed lines in Figure 8 (b). The cooperative diffusion observed in the semidilute entangled solution (solid triangles in Figure 8 (b)) dominates the autocorrelation function on the same time scale as intramolecular chain relaxations in the case of a dilute solution (solid squares in Figure 8 (b)). Hence one may conclude that upon increasing the polymer concentration the contribution of internal chain motions to the single chain dynamics decreases while the contribution of the cooperative motions increases because of the fluctuations of the surrounding polymer chains. Both types of dynamics are observable on the same time scale but in different concentration regimes for high molecular weight PS chains. In the case of internal chain motions the dynamics is driven by fluctuations of the solvent while fluctuations of the surrounding polymer network induce the cooperative dynamics. The fact that cooperative diffusion and internal chain motions occur on similar time and length scales has already been discussed earlier (see ref⁸⁹ and references therein).

Without entanglements the local concentration fluctuations at low scattering vectors \mathbf{q} are suppressed by the osmotic pressure of the solution, and the total dynamic scattering function $S_{tot}(q, \phi, \tau)$ measured by DLS decays via cooperative diffusion according to eqs 16 - 18. However, in the presence of entanglements, there is an additional suppression of concentration fluctuations. Some concentration fluctuations may be frozen in by the entanglements.⁹⁰⁻⁹² This fraction of light scattering signal may only decay with the spectrum of relaxation times of the entanglements themselves, leading to a slow relaxation of the total dynamic scattering function as is shown in Figures 9 (a) and (b) for the 67 kg/Mol and 515 kg/Mol PS chains in semidilute entangled solution at $c=13\%$ wt (solid triangles). The corresponding upper solid lines in Figures 9 (a) and (b) have been calculated according to

$$S_{tot}(q, \phi, \tau) = S_c(q, \phi) \exp(-q^2 D_c \tau) + S_{sl}(q, \phi) \exp(-\tau/\tau_{sl}), \quad (27)$$

where τ_{sl} is a decay time. For arbitrary values of the magnitude of the scattering vector q and the volume fraction ϕ , the shape of the total dynamic scattering function $S_{tot}(q, \phi, \tau)$ is more complex than the expression given in eq 27. For large values of q intramolecular motions lead to a stretched exponential decay of $S_{tot}(q, \phi, \tau)$ for short times (see e.g., refs^{77,78}). Moreover, the contribution of the slow relaxation to $S_{tot}(q, \phi, \tau)$ is in general given by a linear combination of exponentially decaying functions, i.e., $\sum_i \exp(-\tau/\tau_{i,d})$.^{93,94}

Experiments on PS in various solvents have confirmed that the slow relaxation can be measured using DLS.⁹⁵⁻¹⁰³ However, the microscopic understanding of the slow relaxation needs to be improved.¹⁰⁴ On the basis of our FCS and DLS measurements shown in Fig-

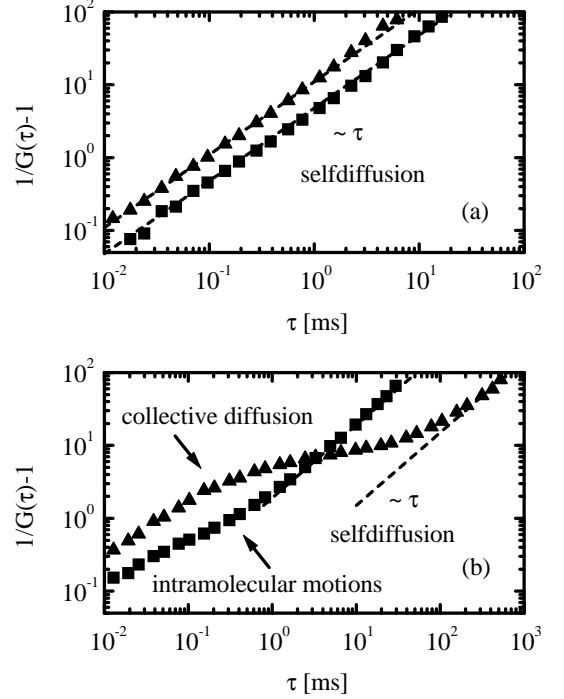


FIG. 8: The FCS autocorrelation function $1/G(\tau) - 1$ of 17 kg/Mol polystyrene chains (a) and 515 kg/Mol polystyrene chains (b) in dilute solution (\blacksquare , $c \rightarrow 0$) and in semidilute solution (\blacktriangle , $c = 13\%$). The dashed lines of slope τ characterize self-diffusion. Intramolecular motions and cooperative diffusion dominate in dilute and semidilute entangled solution, respectively, for short times in the case of the high molecular weight polystyrene chains in (b).

ures 8 and 9 we note that self-diffusion (D_s) occurs on an intermediate time scale, i.e., $1/(q^2 D_c) = 0.05$ ms, $1/(q^2 D_s) = 16$ ms, and $\tau_{sl} = 1087$ ms for $q = 157.6 \mu\text{m}^{-1}$ for the 515 kg/Mol PS chains. For comparison Figures 9 (a) and (b) also display the measured total dynamic scattering function of the PS chains in semidilute unentangled solution (solid squares). In this case there is no slow relaxation due to insufficient chain overlap. The corresponding lower solid lines in Figures 9 (a) and (b) have been calculated according to eq 27 with $S_{sl}(q, \phi) = 0$.

The direct DLS measurement of the slow relaxation confirms our earlier remark that cooperative diffusion becomes highly correlated in the transient entanglement network and can be studied using only a small fraction of labeled polymer chains within FCS. As is illustrated in Figure 10 (b) unlabeled polymer chains (see, e.g., the polymer chain denoted by the index 1) and labeled polymer chains (see, e.g., the polymer chain denoted by the index 2) move in a coherent manner due to entanglements into the FCS observation volume enclosed by the grey ellipsoidal lines. The resulting temporal fluctuations of fluorescence light emitted by labeled polymer chains can be detected by FCS in terms of the cooperative diffusion.

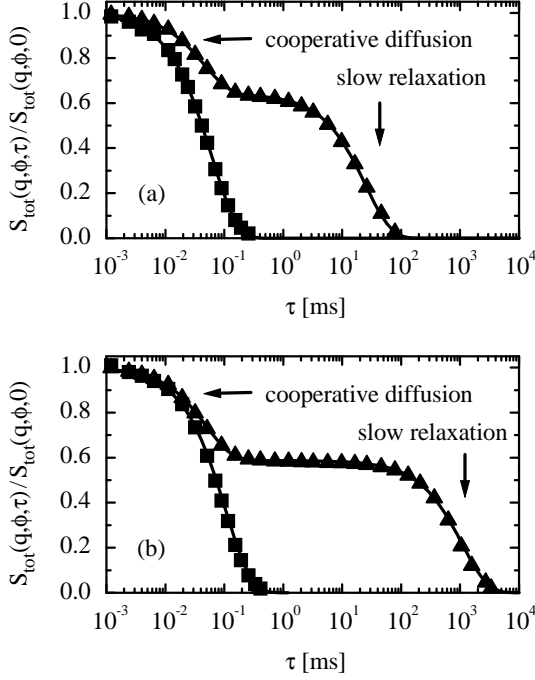


FIG. 9: The total dynamic scattering function $S_{tot}(q, \phi, \tau)$ of 67 kg/Mol polystyrene chains (a) and 515 kg/Mol polystyrene chains (b) measured by DLS in semidilute unentangled solution (\blacksquare , $c = 1$ wt %) and in semidilute entangled solution (\blacktriangle , $c = 13$ wt %). The solid lines follow from eq 27. For short times cooperative diffusion dominates, while the slow relaxation dominates for very large times in semidilute entangled solution. There is no slow relaxation in semidilute unentangled solution, i.e., $S_{sl}(q, \phi) = 0$ in eq 27. The absolute value of the scattering vector is given by $q = 157.6 \mu\text{m}^{-1}$.

A spherical volume of mean size equivalent to the radius of gyration of an individual polymer chain contains about 15 polymer chains at the concentration c^+ at which cooperative diffusion is measured with FCS. Consequently, neighbouring chains strongly interpenetrate and entangle with each other leading to highly cooperative motions in this correlated state. Without entanglements cooperative diffusion cannot be detected if only a small fraction of the polymer chains are labeled due to insufficient chain overlap. Hence in dilute and semidilute unentangled solutions the unlabeled polymer chain denoted by 1 in Figure 10 (a) moves from left to right into the FCS observation volume nearly without influencing the remaining labeled and unlabeled polymer chains.

F. Onset of glassy dynamics

Upon approaching the glass transition concentration $c_{gl} \approx 80$ wt % of PS in toluene,^{53,105} the dynamics of the polymer chains slows down considerably (see ref¹⁰⁶ and references therein). A first signature of this slowing down

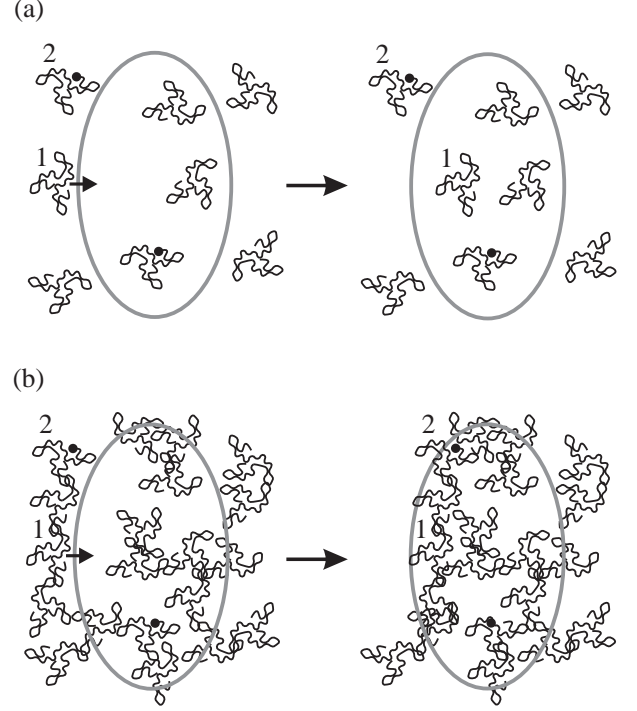


FIG. 10: Schematic illustration of the cooperative diffusion process which is related to the relaxation of the total polymer number density towards the average total number density. The polymer chain denoted by the index 1 moves in (a) and (b) from left to right into the FCS observation volume enclosed by the grey ellipsoidal lines. The polymer chain diffuses into the observation volume nearly without influencing the locations of the remaining polymer chains in an unentangled solution in (a), while the motion of the polymer chain leads to coherent movement of the surrounding polymer chains in semidilute entangled solution in (b). The size of the polymer chains, the size observation volume, and the number of polymer chains are not drawn to absolute scale. Only the fact that in (b) the motion of the unlabeled polymer chain denoted by the index 1 induces a correlated movement of the labeled polymer chain denoted by the index 2 into the observation volume is relevant. Each labeled polymer chain carries only one dye molecule at one of its ends which is marked by a black dot. As the labeled polymer chain denoted by the index 2 diffuses into the observation volume from left to right in (b), it causes temporal fluctuations of the detected fluorescence intensity which can be measured by FCS even in the case that the number of labeled polymer chains is considerably smaller than the number of unlabeled polymer chains. In addition self-diffusion can be measured using FCS both in (a) and (b) as discussed in Section IV A. In (b) self-diffusion of polymer chains corresponds to movements of the polymer chains along their contour through the transient network.

is given by the deviations of the measured cooperative diffusion coefficients D_c from the solid line at high concentrations in fig 7. The cooperative diffusion coefficient decreases by more than three decades as compared to its

maximum value upon further increasing the concentration (see fig 6 in ref⁵³). A second signature of the onset of glassy dynamics is given by the shape of the autocorrelation function $G(\tau)$ measured with FCS. Figure 11 displays measured functions $1/G(\tau) - 1$ (solid symbols) for the 515 kg/Mol PS chains at three concentrations $c = 9.1, 13$, and 20 wt % together with the autocorrelation function for the highest concentration (solid line) calculated according to eq 5 with eq 3 and

$$\phi_s(\tau) = 6D_s\tau + A_s\tau^\beta, \quad \beta = 0.3. \quad (28)$$

Subdiffusive motion characterized by the stretching parameter β is observed as an additional mode on an intermediate time scale between the fast cooperative diffusion (D_c) and the slow self-diffusion (D_s). The dotted line in fig 11 represents the asymptotic shape of $1/G(\tau) - 1$ in the intermediate time regime. Both the exponent $\beta = 0.3$ and the time scale agree with literature values for PS.^{53,107}

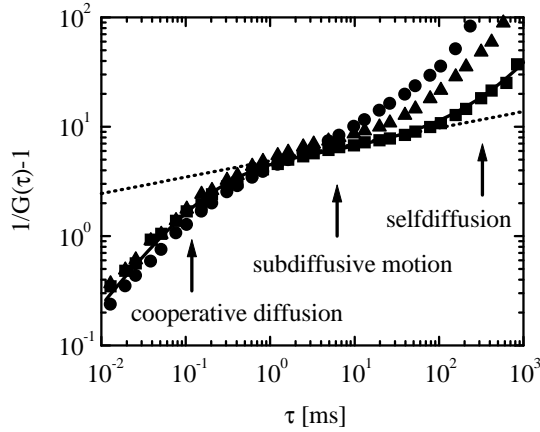


FIG. 11: The measured FCS autocorrelation function $1/G(\tau) - 1$ of a 515 kg/Mol polystyrene solution at three concentrations: $c = 9.1$ wt %, (\bullet); $c = 13$ wt %, (\blacktriangle); $c = 20$ wt %, (\blacksquare). The solid line displays the result for the highest concentration as obtained from eq 5 with eqs 4 and 28 as input. For short and large times cooperative diffusion and self-diffusion dominate, respectively. The dotted line represents the asymptotic shape of the autocorrelation function in the intermediate time regime.

V. AN APPLICATION: COMPARISON WITH MINIMUM CONCENTRATION REQUIRED TO PRODUCE NANOFIBERS

The understanding of dynamical properties of semidilute entangled polymer solutions is also important for various technological relevant applications. As an example we discuss the formation of nanofibers from polymer solutions. Polymer nanofibers are attractive building blocks for functional nanoscale devices. They are

promising candidates for various applications, including filtration, protective clothing, polymer batteries, sensors, and tissue engineering.^{108,109} Electrospinning is one of the most established fiber fabrication methods and has attracted much attention due to the ease by which nanofibers can be produced from polymer solutions.¹¹⁰ Fibers produced by this approach are at least one or two orders of magnitude smaller in diameter than those produced by conventional fiber production methods like melt or solution spinning. In a typical electrospinning process a jet is ejected from the surface of a charged polymer solution when the applied electric field strength overcomes the surface tension. The ejected jet travels rapidly to the collector target located at some distance from the charged polymer solution under the influence of the electric field and becomes collected in the form of a solid polymer nanofiber. However, this method requires a dc voltage in the kV range and high fiber production rates are difficult to achieve because only a single fiber emerges from the nozzle of the pipet holding the polymer solution.¹¹⁰ In order to overcome these deficiencies an efficient procedure enabling the parallel fabrication of a multitude of polymer fibers with regular morphology and diameters as small as 25 nm has been reported recently.¹¹¹ It involves the application of drops of a polymer solution onto a standard spin coater, followed by fast rotation of the chuck, without the need of a mechanical constriction. The fiber formation relies upon the instability of the spin-coated liquid film that arises due to a competition of the centrifugal force and the Laplace force induced by the surface curvature. This Rayleigh-Taylor instability triggers the formation of thin liquid jets emerging from the outward driven polymer solution, yielding solid nanofibers after evaporation of the solvent.

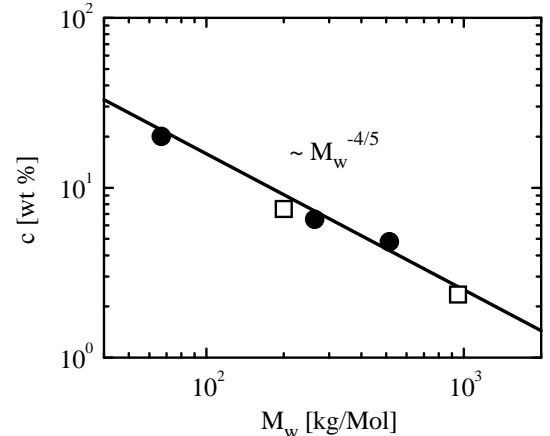


FIG. 12: The concentration c^+ (\bullet) at which the cooperative diffusion mode appears in the FCS measurements together with the minimum concentration c_{fib} (\square) required to produce nanofibers¹¹¹ as a function of the molecular weight M_w . The solid line of slope $M_w^{-4/5}$ represents a scaling relation valid for polymers in a good solvent.

The reason why the ejected jets of polymer solution do not further break up into individual droplets, but rather give rise to continuous, solid nanofibers, is related to the dynamic properties of the polymer solutions. In order to elucidate this point in more detail, Figure 12 displays the minimum concentration c_{fib} required to produce nanofibers from 200 kg/Mol and 950 kg/Mol poly-(methylmethacrylate) solution (open squares)¹¹¹ together with the concentration c^+ at which the cooperative diffusion mode appears in the FCS measurements of the 67 kg/Mol, 264 kg/Mol, and 515 kg/Mol PS solutions (solid circles). Interestingly, the concentrations c_{fib} and c^+ follow approximately the same scaling relationship $c_{fib} = c^+ \sim M_w^{-4/5}$ (c.f., eq 13). Hence, the nanofiber formation requires that the polymer concentration exceeds the concentration c^+ where basically all molecules are involved in the correlated cooperative dynamics. Uniform fibers cannot be obtained for lower concentrations due to insufficient chain overlap and the dominating self-diffusion which leads to a disentanglement under the influence of external forces such as the centrifugal force or the electrostatic force.

VI. CONCLUSION

A general analysis of the diffusion in polystyrene solutions obtained by fluorescence correlation spectroscopy and by dynamic light scattering has been presented. Two different diffusion coefficients have been obtained with fluorescence correlation spectroscopy using single-labeled polystyrene in toluene solutions [Figures 1 - 4]. The self-diffusion coefficient D_s results from fluorescence correlation spectroscopy in the limit of small concentrations of labeled molecules and for arbitrary concentrations of unlabeled molecules. Moreover, the cooperative diffusion coefficient D_c in the semidilute entangled regime becomes accessible as well which is ascribed to an **effective** long-range interaction of the labeled chains in the transient entanglement network. The self-diffusion coefficients D_s can be determined from the cooperative diffusion coefficient

D_c obtained by dynamic light scattering measurements and vice versa according to eqs 8 and 9.

The measurements verify the basic scaling and reptation theory for semidilute entangled polymer solutions [Figures 3, 5, 6 and eqs 10, 12, 14]. A quantitative basis for the modelling of the cooperative diffusion coefficient is given by a Langevin and generalized Ornstein-Zernike equation [eqs 15 - 23]. The calculated cooperative diffusion coefficients agree with the measured results both in the dilute and semidilute regimes [Figure 7]. In particular the features of the crossover region between the dilute and the semidilute regimes are captured correctly by the underlying integral equation theory.

For large times the decay of the fluorescence correlation spectroscopy autocorrelation function is dominated by self-diffusion, while intramolecular chain relaxations in dilute solution and cooperative diffusion in semidilute entangled solution dominate for short times [Figures 6 and 8]. An additional slow relaxation in semidilute entangled solution can be observed by dynamic light scattering [Figure 9]. Moreover, the fluorescence correlation spectroscopy autocorrelation function exhibits an additional mode on an intermediate time scale upon approaching the glass transition concentration [Figure 11].

Finally, it has been shown the minimum concentration required to produce solid nanofibers from a polymer solution follows the same scaling relationship as the concentration at which the cooperative diffusion mode appears in the fluorescence correlation spectroscopy measurements [Figure 12]. The nanofiber formation requires that the polymer concentration exceeds the concentration where basically all molecules are involved in the correlated cooperative dynamics. Hence fluorescence correlation spectroscopy is helpful for the understanding of dynamical properties of semidilute entangled polymer solutions in the case of technological relevant applications.

We thank A. H. E. Müller and A. Böker for the synthesis of the polymers and the Deutsche Forschungsgemeinschaft, SFB 481 (A11), Bayreuth, for financial support.

* Electronic address: Matthias.Ballauff@uni-bayreuth.de

¹ De Gennes, P.-G. *Scaling Concepts in Polymer Physics*; Cornell University Press: Ithaca, N.Y., 1979.

² Doi, M.; Edwards, S. F. *The Theory of Polymer Dynamics*; Clarendon Press: Oxford, 1986.

³ Adam, M.; Delsanti, M. *Macromolecules* **1977**, *10*, 1229.

⁴ Cosgrove, T.; Sutherland, J. M. *Polymer* **1983**, *24*, 534.

⁵ Brown, W.; Zhou, P. *Macromolecules* **1991**, *24*, 5151.

⁶ Le Bon, C.; Nicolai, T.; Kuil, M. E.; Hollander, J. G. *J. Phys. Chem. B* **1999**, *103*, 10294.

⁷ Kanematsu, T.; Sato, T.; Imai, Y.; Ute, K.; Kitayama, T. *Polymer J.* **2005**, *37*, 65.

⁸ Pecora, R. *Dynamic light scattering*; Plenum Press: New York, 1985.

⁹ Min, G.; Savin, D.; Gu, Z.; Patterson, G. D.; Kim, S. H.; Ramsay, D. J.; Fishman, D.; Ivanov, I.; Sheina, E.; Slaby, E.; Oliver, J. *Int. J. Pol. Anal. Charact.* **2003**, *8*, 187.

¹⁰ Hervet, H.; Léger, L.; Rondelez, F. *Phys. Rev. Lett.* **1979**, *42*, 1681.

¹¹ Zettl, H.; Häfner, W.; Böker, A.; Schmalz, H.; Lanzendörfer, M.; Müller, A. H. E.; Krausch, G. *Macromolecules* **2004**, *37*, 1917.

¹² Zettl, H.; Zettl, U.; Krausch, G.; Enderlein, J.; Ballauff, M. *Phys. Rev. E* **2007**, *75*, 061804.

¹³ Liu, R. G.; Gao, X.; Adams, J.; Oppermann, W. *Macromolecules* **2005**, *38*, 8845.

¹⁴ Bier, M.; van Roij, R.; Dijkstra, M.; van der Schoot, P. *Phys. Rev. Lett.* **2008**, *101*, 215901.

- ¹⁵ Michelman-Riberiro, A.; Boukari, H.; Nossal, R.; Horkay, F.; *Macromolecules* **2004**, *37*, 10212.
- ¹⁶ Gianneli, M.; Beines, P. W.; Roskamp, R. F.; Koynov, K.; Fytas, G.; Knoll, W. *J. Phys. Chem. C* **2007**, *111*, 13205.
- ¹⁷ Cherdhirankorn, T.; Best, A.; Koynov, K.; Peneva, K.; Muellen, K.; Fytas, G. *J. Phys. Chem. B* **2009**, *113*, 3355.
- ¹⁸ Grabowski, C. A.; Mukhopadhyay, A. *Macromolecules* **2008**, *41*, 6191.
- ¹⁹ Scalettar, B. A.; Hearst, J. E.; Klein, M. P. *Macromolecules* **1989**, *22*, 4550.
- ²⁰ Rička, J.; Binkert, T. *Phys. Rev. A* **1989**, *39*, 2646.
- ²¹ Zettl, H.; Portnoy, Y.; Gottlieb, M.; Krausch, G. *J. Phys. Chem. B* **2005**, *109*, 13397.
- ²² Kniewske, R.; Kulicke, W. M. *Macromol. Chem.* **1983**, *184*, 2173.
- ²³ Rigler, R.; Elson, E. S. *Fluorescence Correlation Spectroscopy: Theory and Applications*; Springer: Heidelberg, 2001.
- ²⁴ Wahl, M.; Koberling, F.; Patting, M.; Rahn, H.; Erdmann, R. *Curr. Pharm. Biotechnol.* **2004**, *5*, 299.
- ²⁵ Enderlein, J.; Gregor, I. *Rev. Sci. Instr.* **2005**, *76*, 033102.
- ²⁶ Magde, D.; Elson, E.; Webb, W. W. *Phys. Rev. Lett.* **1972**, *29*, 705.
- ²⁷ Pusey, P. N.; Fijnaut, H. M.; Vrij, A. *J. Chem. Phys.* **1982**, *77*, 4270.
- ²⁸ Akcasu, A. Z.; Nägele, G.; Klein, R. *Macromolecules* **1991**, *24*, 4408.
- ²⁹ Kirkwood, J. G.; Riseman, J. *J. Chem. Phys.* **1948**, *16*, 565.
- ³⁰ Fujita, H. *Polymer Solutions*; Elsevier: Amsterdam, 1990.
- ³¹ Kim, H.; Chang, T.; Yohanan, J. M.; Wang, L.; Yu, H. *Macromolecules* **1986**, *19*, 2737.
- ³² Schulz, G. V.; Hoffmann, M. *Macromol. Chem.* **1957**, *23*, 220.
- ³³ Lodge, T. P.; Rotstein, N. A.; Prager, S. *Adv. Chem. Phys.* **1990**, *79*, 1.
- ³⁴ McLeish, T. C. B. *Adv. Phys.* **2002**, *51*, 1379.
- ³⁵ Léger, L.; Hervet, H.; Rondelez, F. *Macromolecules* **1981**, *14*, 1732.
- ³⁶ King, T. A.; Knox, A.; McAdam, J. D. G. *Polymer* **1973**, *14*, 293.
- ³⁷ Harnau, L.; Winkler, R. G.; Reineker, P. *J. Chem. Phys.* **1995**, *102*, 7750.
- ³⁸ Harnau, L.; Winkler, R. G.; Reineker, P. *J. Chem. Phys.* **1998**, *109*, 5160.
- ³⁹ Harnau, L.; Winkler, R. G.; Reineker, P. *Phys. Rev. Lett.* **1999**, *82*, 2408.
- ⁴⁰ Harnau, L.; Winkler, R. G.; Reineker, P. *Europhys. Lett.* **1999**, *45*, 488.
- ⁴¹ Lumma, D.; Keller, S.; Vilgis, T.; Rädler, J. O. *Phys. Rev. Lett.* **2003**, *90*, 218301.
- ⁴² Shusterman, R.; Alon, S.; Gavrinov, T.; Krichevsky, O. *Phys. Rev. Lett.* **2004**, *92*, 048303.
- ⁴³ Bernheim-Groswasser, A.; Shusterman, R.; Krichevsky, O. *J. Chem. Phys.* **2006**, *125*, 084903.
- ⁴⁴ Petrov, E. P.; Ohrt, T.; Winkler, R. G.; Schwille, P. *Phys. Rev. Lett.* **2006**, *97*, 258101.
- ⁴⁵ Winkler, R. G.; Keller, S.; Rädler, J. O. *Phys. Rev. E* **2006**, *73*, 041919.
- ⁴⁶ Shusterman, R.; Gavrinov, T.; Krichevsky, O. *Phys. Rev. Lett.* **2008**, *100*, 098102.
- ⁴⁷ Kremer, K.; Binder, K. *J. Chem. Phys.* **1984**, *81*, 6381.
- ⁴⁸ Paul, W.; Binder, K.; Heermann, D. W.; Kremer, K. *J. Phys. II (France)* **1991**, *1*, 37.
- ⁴⁹ Harnau, L.; Reineker, P. *Phys. Rev. E* **1999**, *60*, 4671.
- ⁵⁰ Wiltzius, P.; Haller, H. R.; Cannell, D. S.; Schaeffer, D. W. *Phys. Rev. Lett.* **1984**, *53*, 834.
- ⁵¹ Nemoto, N.; Makita, Y.; Tsunashima, Y.; Kurata, M. *Macromolecules* **1984**, *17*, 2629.
- ⁵² Zhang, K. J.; Briggs, M. E.; Gammon, R. W.; Sengers, J. V.; Douglas, J. F. *J. Chem. Phys.* **1999**, *111*, 2270.
- ⁵³ Rauch, J.; Köhler, W. *J. Chem. Phys.* **2003**, *119*, 11977.
- ⁵⁴ Geissler, E.; Hecht, A. M. *J. Phys. (France) Lett.* **1978**, *39*, 631.
- ⁵⁵ Brown, W.; Nicolai, T. *Colloid. Polym. Sci.* **1990**, *268*, 977.
- ⁵⁶ Schweizer, K. S.; Curro, J. G. *Adv. Chem. Phys.* **1997**, *98*, 1.
- ⁵⁷ Harnau, L. *Molec. Phys.* **2008**, *106*, 1975.
- ⁵⁸ Yethiraj, A. *J. Phys. Chem. B* **2009**, *113*, 1539.
- ⁵⁹ Harnau, L. *J. Chem. Phys.* **2001**, *115*, 1943.
- ⁶⁰ Bolisetty, S.; Airaud, C.; Xu, Y.; Müller, A. H. E.; Harnau, L.; Rosenfeldt, S.; Lindner, P.; Ballauff, M. *Phys. Rev. E* **2007**, *75*, 040803(R).
- ⁶¹ Bolisetty, S.; Rosenfeldt, S.; Rochette, C. N.; Harnau, L.; Lindner, P.; Xu, Y.; Müller, A. H. E.; Ballauff, M. *Colloid. Polym. Sci.* **2009**, *287*, 129.
- ⁶² Rosenfeldt, S.; Karpuk, E.; Lehmann, M.; Meier, H.; Lindner, P.; Harnau, L.; Ballauff, M. *ChemPhysChem* **2006**, *7*, 2097.
- ⁶³ Harnau, L.; Rosenfeldt, S.; Ballauff, M. *J. Chem. Phys.* **2007**, *127*, 014901.
- ⁶⁴ Yethiraj, A.; Shew, C.-Y. *Phys. Rev. Lett.* **1996**, *77*, 3937.
- ⁶⁵ Yethiraj, A.; Shew, C.-Y. *J. Chem. Phys.* **1997**, *106*, 5706.
- ⁶⁶ Shew, C.-Y.; Yethiraj, A. *J. Chem. Phys.* **1998**, *109*, 5162.
- ⁶⁷ Harnau, L.; Reineker, P. *J. Chem. Phys.* **2000**, *112*, 437.
- ⁶⁸ Harnau, L.; Costa, D.; Hansen, J.-P. *Europhys. Lett.* **2001**, *53*, 729.
- ⁶⁹ Harnau, L.; Hansen, J.-P. *J. Chem. Phys.* **2002**, *116*, 9051.
- ⁷⁰ Weber, C. H. M.; Chiche, A.; Krausch, G.; Rosenfeldt, S.; Ballauff, M.; Harnau, L.; Göttker-Schnetmann, I.; Tong, Q.; Mecking, S. *Nano Letters* **2007**, *7*, 2024.
- ⁷¹ Henzler, K.; Rosenfeldt, S.; Wittemann, A.; Harnau, L.; Narayanan, T.; Ballauff, M. *Phys. Rev. Lett.* **2008**, *100*, 158301.
- ⁷² Fuchs, M.; Schweizer, K. S. *J. Chem. Phys.* **1997**, *106*, 347.
- ⁷³ Daoud, M.; Cotton, J. P.; Farnoux, B.; Jannink, G.; Sarma, G.; Benoit, H.; Duplessix, R.; Picot, C.; De Gennes, P.-G. *Macromolecules* **1975**, *8*, 804.
- ⁷⁴ Fetters, L. J.; Hadjichristidis, N.; Lindner, J. S.; Mays, J. W. *J. Phys. Chem. Ref. Data* **1994**, *23*, 619.
- ⁷⁵ Terao, K.; Mays, J. W. *Eur. Polym. J.* **2004**, *40*, 1623.
- ⁷⁶ Rotne, J.; Prager, S. *J. Chem. Phys.* **1969**, *50*, 4831.
- ⁷⁷ Harnau, L.; Winkler, R. G.; Reineker, P. *J. Chem. Phys.* **1996**, *104*, 6355.
- ⁷⁸ Harnau, L.; Winkler, R. G.; Reineker, P. *Macromolecules* **1999**, *32*, 5956.
- ⁷⁹ Harnau, L.; Winkler, R. G.; Reineker, P. *J. Chem. Phys.* **1997**, *106*, 2469.
- ⁸⁰ Schweizer, K. S. *J. Chem. Phys.* **1989**, *91*, 5822.
- ⁸¹ Semenov, A. N. *Physica A* **1991**, *171*, 517.
- ⁸² Genz, U. *Macromolecules* **1994**, *27*, 6452.
- ⁸³ Schweizer, K. S.; Fuchs, M.; Szamel, G.; Guenza, M.; Tang, H. *Macromol. Theory Simul.* **1997**, *6*, 1037.

- ⁸⁴ Guenza, M. *J. Phys. Chem.* **1999**, *110*, 7574.
- ⁸⁵ Semenov, A. N.; Rubinstein, M. *Eur. Phys. J. B.* **1998**, *1*, 87.
- ⁸⁶ Altukhov, Y. A.; Pokrovskii, V. N.; Pyshnogra, G. V. *J. Non-Newtonian Fluid Mech.* **2004**, *121*, 73.
- ⁸⁷ Pokrovskii, V. N. *Physica A* **2006**, *366*, 88.
- ⁸⁸ Pokrovskii, V. N. *J. Expt. Theo. Phys.* **2008**, *106*, 604.
- ⁸⁹ Jian, T.; Vlassopoulos, D.; Fytas, G.; Pakula, T.; Brown, W. *Colloid Polym. Sci.* **1996**, *274*, 1033.
- ⁹⁰ Brochard, F.; De Gennes, P. G. *Macromolecules*, **1977**, *10*, 1157.
- ⁹¹ Doi, M.; Onuki, A. *J. Phys. II (France)*, **1992**, *2*, 1631.
- ⁹² Einaga, Y.; Fujita, H. *Polymer*, **1999**, *40*, 565.
- ⁹³ Einaga, Y.; Itaya, A.; Takaoka, M. *Polymer*, **2002**, *43*, 4869.
- ⁹⁴ Takenaka, M.; Nishitsuji, S.; Hasegawa, H. *J. Phys. Chem.*, **2007**, *126*, 064903.
- ⁹⁵ Brown, W.; Nicolai, T.; Hvidt, S.; Stepanek, P. *Macromolecules*, **1990**, *23*, 357.
- ⁹⁶ Nicolai, T.; Brown, W.; Johnsen, R. M.; Stepanek, P. *Macromolecules*, **1990**, *23*, 1165.
- ⁹⁷ Nicolai, T.; Brown, W. *Macromolecules*, **1990**, *23*, 3150.
- ⁹⁸ Nicolai, T.; Brown, W.; Hvidt, S.; Heller, K. *Macromolecules*, **1990**, *23*, 5088.
- ⁹⁹ Wang, C. H.; Zhang, X. Q. *Macromolecules*, **1993**, *26*, 707.
- ¹⁰⁰ Brown, W.; Stepanek, P. *Macromolecules*, **1993**, *26*, 6884.
- ¹⁰¹ Sun, Z.; Wang, C. H. *Macromolecules*, **1994**, *27*, 5667.
- ¹⁰² Wang, C. H.; Zhang, X. Q. *Macromolecules*, **1995**, *28*, 2288.
- ¹⁰³ Lin, C.-N.; Song, Y.-M.; Yu, T.-L. *J. Polym. Res.*, **1997**, *4*, 107.
- ¹⁰⁴ Li, J.; Li, W.; Huo, H.; Luo, S.; Wu, C. *Macromolecules*, **2008**, *41*, 901.
- ¹⁰⁵ Konak, C.; Brown, W. *J. Chem. Phys.* **1993**, *98*, 9014.
- ¹⁰⁶ Peter, S.; Meyer, H.; Baschnagel, J. *Eur. Phys. J. E.* **2009**, *28*, 147.
- ¹⁰⁷ Lindsey, C.; Patterson, G.; Stevens, J. *J. Polym. Sci., Polym. Phys. Ed.* **1979**, *17*, 1547.
- ¹⁰⁸ Ramakrishna, S.; Fujihara, K.; Teo, W.-E.; Lim, T.-C.; Ma, Z. *Introduction to Electrospinning and Nanofibers*; World Scientific: Singapore, 2005.
- ¹⁰⁹ Stevens, M.; George, M. *Science* **2005**, *310*, 1135.
- ¹¹⁰ Greiner, A.; Wendorff, J. H. *Angew. Chem. Int. Ed.* **2007**, *46*, 5670.
- ¹¹¹ Weitz, R. T.; Harnau, L.; Rauschenbach, S.; Burghard, M.; Kern, K. *Nano Lett.* **2008**, *8*, 1187.